High-sorption terpyridine–graphene oxide hybrid for the efficient removal of heavy metal ions from wastewater

Dawid Pakulski, Adam Gorczyński, Dawid Marcinkowski, Wlodzimierz Czepa, Tomasz Chudziak, Samanta Witomska, Yuta Nishina, Violetta Patroniak, Artur Ciesielski, Paolo Samorì

ARTICLE

High-sorption terpyridine-graphene oxide hybrid for efficient removal of heavy metal ions from wastewater

Received 00th January 20xx,
Accepted 00th January 20xx

DOI: 10.1039/x0xx00000x

Dawid Pakulski,*[a,b] Adam Gorczyński,[a] Dawid Marcinkowski,[a] Włodzimierz Czepa,[a] Tomasz Chudziak,[a] Samanta Witomska,[a] Yuta Nishina,[c] Violetta Patroniak,[a] Artur Ciesielski,*[b,d] and Paolo Samorì *[d]

Pollution of wastewater with heavy metal-ions represents one of the most severe environmental problems associated with the societal development. To overcome this issue, the design of new, highly efficient systems capable to remove such poisoning species, hence to purify water, is of paramount importance for public health and environmental protection. In this work, novel sorption hybrid materials were developed to enable high-performance adsorption of heavy metal ions. Towards this end, graphene oxide (GO) exhibiting various C/O ratios has been functionalized with ad hoc receptors, i.e. terpyridine ligands. The maximum adsorption capacity of highly oxidized/terpyridine hybrids towards Ni(II), Zn(II) and Co(II) were achieved at pH=6 and 25°C reaching values of 462, 421 and 336 mg g^{-1}, respectively, being the highest reported in the literature for pristine GO and GO-based sorbents. Moreover, the uptake experiments showed that the GO–Tpy as well as GO_h-Tpy adsorption of heavy metal ions is strongly dependent on the pH in the range from 2 to 10, as a result of the modulation of interactions at the supramolecular level. Moreover, the ionic strength was found being independent of heavy metal ions adsorption on GO-Tpy and GO_h-Tpy. Under ambient conditions, adsorption capacity values increase with the degree of oxidation of GO because dipolar oxygen units can both interact with heavy-metal ions via dipole-dipole and/or ionic interactions and they enable higher amount of covalently-anchored terpyridine units. Both the adsorption isotherms and kinetics studies revealed that the uptake of the heavy metal ions occurs at a monolayer coverage, mostly controlled by the strong surface complexation with the oxygen of GO and terpyridine nitrogen-containing groups. Furthermore, selectivity of the hybrid was confirmed by selective sorption of the above heavy metal ions from mixtures involving alkali (Na(I), K(I)) and alkaline earth (Mg(II), Ca(II)) metal ions due to the chelating properties of the terpyridine subunits, as demonstrated on a municipal drinking (tap) water samples. Our findings provide unambiguous evidence for the potential of chemical tailoring of GO-based materials with N-heterocyclic ligands for highly efficient wastewater purification sorbent materials.

Introduction

One of the most detrimental downsides of the rapid industrial development is associated with its impact on the environment.[1, 2] The increasing use of heavy metals for numerous applications in metallurgy, mining or chemical and battery manufacturing is highly relevant since it is the major source of the pollution of water reservoirs.[3-5] This originates the bioaccumulation of heavy metal ions in the food chains, thereby compromising the ability to foster animal and plant life.[6, 7] Their accumulation in human bodies results in the deterioration of the overall health, affecting all vital organs and eventually leading to chronic illnesses, overall lifespan shortening and, in worst-case scenario, premature death.[8, 9]

The most economically viable and therefore industrially applied methods for wastewater treatment are based on the adsorption techniques, usually in the form of membranes employed in desalination or chemisorption setups.[10-14] Over many years, researchers have explored the effectiveness of various adsorbents in these processes, including activated carbon (AC), zeolites, covalent organic frameworks (COFs), polymers, biosorbents, and other low-cost materials.[15-27] However, practical application of these systems is limited due to low adsorption capacities, problematic separation and poor recyclability, yielding an overall limited effectiveness. As a result, tremendous effort has been made in recent years to design and develop new sorption materials towards enhanced sorption capacity; towards this end, graphene-based materials were shown to be the extremely effective for this application.[28-31] For example, Seo and co-workers demonstrated the applicability of graphene-based membranes for desalination of

[a] Faculty of Chemistry, Adam Mickiewicz University, Uniwersytetu Poznańskiego 8, 61-614 Poznań, Poland.
[b] Center for Advanced Technologies Adam Mickiewicz University, Uniwersytetu Poznańskiego 10, 61-614 Poznań, Poland.
[c] Research Core for Interdisciplinary Sciences, Okayama University, 3-1-1 Tsushimanaka, Kita-ku, Okayama, 700-8530, Japan.
[d] Université de Strasbourg, CNRS, ISIS 8 allée Gaspard Monge, 67000 Strasbourg, France.

E-mail: dawid.pakulski@amu.edu.pl, ciesielski@unistra.fr, samori@unistra.fr

† Electronic Supplementary Information (ESI) available: [details of any supplementary information available should be included here]. See DOI: 10.1039/x0xx00000x

water from Sydney Harbour.[32] The unique properties of two-dimensional materials (2DMs), and in particular their significant chemical stability and their high surface-to-volume ratio determined by their atomic thickness, render them particularly adaptive as adsorbents. Among 2DMs, graphene oxide (GO) can be produced in large scale and exposes on its surface various oxygen containing functional groups (e.g., epoxide, hydroxide and carbonyl) that can *per se* bind metal ions *via* the chelation mechanism and/or electrostatic interaction, and can be used as anchoring points for further chemical functionalizations.[33-35] As a result, GO-based adsorbents are considered as attractive candidates for harvesting pollutants from aqueous solutions.

In the last few years, several works have demonstrated the huge potential of GO and modified GO-based materials in sorption process towards different organic and inorganic pollutants,[36] and revealed the impressive adsorption properties towards heavy metals ions (*e.g.,* 138-180 mg g^{-1} Ni(II),[37-39] 297-345 mg g^{-1} Zn(II),[40, 41] 21-116 mg g^{-1} Co(II)[42, 43]). Furthermore, it has been shown that the changes in the adsorption capacity and selectivity are strictly correlated with the chemical functionalization GO surface[37, 38, 40-43] and degree of oxidation of graphene oxide.[44, 45] Unfortunately, there are still some limitations that, if solved, can make utilization of GO-based materials in the wastewater-derived adsorption processes a widely applied methodology. In particular, these materials are typically highly dispersible in water, therefore their regeneration and repeated utilization are not economically feasible. To overcome these drawbacks and towards a sustainable approach, an appropriate synthetic route needs to be devised to increase the degree of oxidation in GO. This implies the presence of a greater number of groups that can act as anchoring points for further functionalization, enabling the fine tuning of the material's properties. As a result, the inherent sorption properties would be expected to increase offering a major step forward compared to the current state-of-the art.

Among various supramolecular receptors of heavy-metal ions,[3, 46] multidentate organic ligands and in particular oligopyridines seem to be a perfect choice for enhancement of the sorption of GO-based materials due to their high complexation constants and sensitivity towards this type of analytes.[47-50] In fact, the successful grafting of *N*-heterocyclic ligands to GO materials was already demonstrated,[51-55] however their utilization was limited to energy conversion processes and anticorrosive properties.

Here, we present a modular strategy towards the generation of a novel library of three-dimensional (3D) porous hybrids, constructed from 4-([2,2':6',2''-terpyridin]-4'-yloxy)butan-1-amine (Tpy) and GO with two different degrees of oxidation as presented on Fig. 1. We envisage that the introduction of the Tpy group could serve as an efficient metal-ion scavenger but would also impose in an increase the interlayer spacing between GO sheets, thus enhancing the specific surface area of the material. We have produced GO sheets with different amount of oxygen functionalities which yielded tunable degree of Tpy-functionalization of the GO. These functionalized GO were exploited to quantify the adsorption capacity and unravel the mechanism of Ni(II), Zn(II) and Co(II) sorption, allowing to achieve the highest reported values of the maximum adsorption capacity (q_{max}) within GO and GO-based sorbents (see table S1). Moreover, we demonstrated a high selectivity in the sorption of heavy metal ions from mixtures involving alkali (Na(I), K(I)) and alkaline earth (Mg(II), Ca(II)) metal ions. High stability and reusability of our sorbent materials was also proven, thus providing a very promising strategy towards the generation of novel and more performing sorbent materials for wastewater treatment.

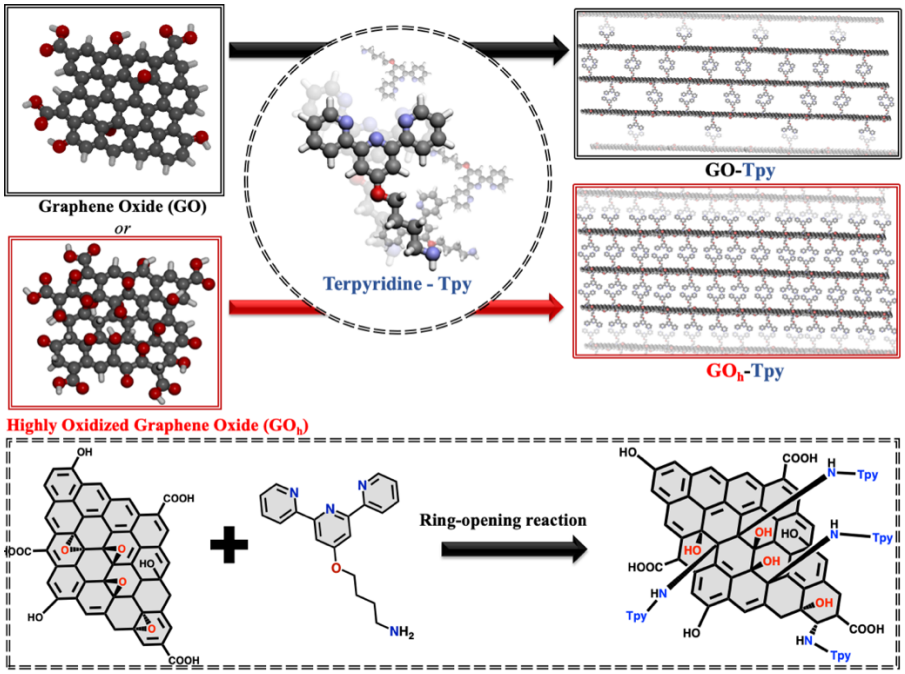

Fig. 1 Schematic representation of the functionalization of graphene oxide with two levels of oxidation (GO and GO_h) with Tpy using ring-opening reaction of epoxides yielding GO-Tpy and GO_h-Tpy.

Results and discussion

Synthesis and characterization of GO-Tpy and GO_h-Tpy hybrids

A family of 3D porous GO-Tpy and GO_h-Tpy hybrids was produced by combining graphene oxides batches differing in the degree of oxidation (GO and GO_h) with tridentate terpyridine ligands (Tpy) (fig. S1) decorated with short amino-alkyl chain for covalent attachment to the GO materials. Overnight reflux, followed by filtration, Soxhlet extraction and freeze-drying allows one to obtain the final material in the pure form in maximum yield with respect to the graphenic system. Such an approach allows one to achieve an efficient decoration of 2D GO surfaces using the pendant amine group of the Tpy scaffold, while retaining the ability of the latter to coordinate heavy metal ions upon its integration into the hybrid material. Careful optimization allowed us to establish that two-fold excess of Tpy with respect to GO/GO_h is the optimum mass ratio to ensure full saturation of the N-heterocyclic material into the carbonaceous matrix. Noteworthy, XPS analysis can provide semiquantitative information concerning the composition,[56] which helped us to estimate the ratio between the number of carbon atoms of graphene oxide over the number of N-heterocyclic moieties (see SI). We calculated the degree of functionalization revealed that GO_h-Tpy possesses two times more Tpy subunits than GO-Tpy. In other words, the higher number of oxygen-containing moieties in GO_h when compared to GO allows more dense grafting of the Tpy moieties onto the material.

The GO, GO_h, GO-Tpy and GO_h-Tpy were investigated by Raman spectroscopy which is a non-destructive and well-established technique used to determine the structure and interaction between components (Fig. S2). The Raman spectra of GO_h and GO_h-Tpy display two characteristic bands which correspond to the D (1340 cm^{-1} for GO_h) and G (1593 cm^{-1} for GO and GO_h; 1584 cm^{-1} for GO-Tpy and GO_h-Tpy) modes. The G band is observed in most of graphite-based materials and it is related to the E_{2G} vibrational mode of ordered in-plane sp^2 hybridized carbon bonds, whereas D band corresponds to the disorder of the edge carbons and is forbidden in an ideal graphite. Compared to GO and GO_h, the G-band of GO-Tpy and GO_h-Tpy appears at 1584 cm^{-1}, being down shifted by 9 cm^{-1}, thereby confirming the charge transfer between GO_h and Tpy units. This is consistent with the observations related to amino-functionalized graphene oxide hybrid,[57] which shows a strong covalent interaction between both components. Typically, chemical modification of graphene-based materials is studied by the changes in the ratio of D and G bands intensities (I_D/I_G).[58-60] When compared to pristine GO (I_D/I_G = 0.95), the I_D/I_G of GO-Tpy becomes higher (I_D/I_G = 1.07) and can be attributed to the increase of sp^3 hybridized carbon atoms after functionalization (Fig. S2). Comparably, after functionalization of Tpy with highly oxidized GO_h, the I_D/I_G increased from 0.96 (for GO_h) to 1.13 for GO_h-Tpy. Fourier transform infrared spectroscopy (FT-IR) further confirmed the covalent modification of GO/GO_h with the Tpy as shown in Fig. S3. Once the Tpy interacts with GO_h, a reaction between amine groups of Tpy with epoxy as well as carbonyl units located on the basal plane of GO_h takes place.[61] Since the strong H-bonding coming from the GO_h essentially overlaps with the characteristic features of the high-energy IR spectrum, changes below 1800 cm^{-1} are proof of successful Tpy functionalization. New bands at 1582 cm^{-1} (N-H bending vibration) and 784 cm^{-1} (N-H out-of-plane wagging mode) in GO-Tpy and GO_h-Tpy spectra demonstrated that the grafting occurred through the amino groups (red dashed lines on Fig. S3)) (also confirmed with XPS study presented below). Characteristic Tpy signals of the sp^2 aromatic counterparts were also present in the final materials (blue dashed lines on Fig. S3), which further confirmed the successful covalent functionalization.

X-ray photoelectron spectroscopy (XPS) analysis was performed to further verify the chemical composition and electronic state of the resulting GO, GO_h, GO-Tpy and GO_h-Tpy (Fig. S4-S5). The important distinction between the carbon (C1s) and nitrogen (N1s) peaks provides evidence for the creation of new chemical bonds between the oxygen containing groups on the surface of GO and amine groups from the Tpy moieties (Fig. S5a-j). Moreover, thanks to this analytical method, we could clearly observe differences in oxidation degree in the GOs used in our work. In particular, the survey spectrum of GO-Tpy and GO_h-Tpy in Fig. S4 show photoelectron lines at a binding energy at ca. 285, 398 and 532 eV which can be attributed to C1s, N1s and O1s peaks, respectively. The C1s XPS spectrum of the neat GO_h (Fig. S5c) shows typical peaks at 284.4 eV (C-C), 286.8 eV (C-O) and peak at 288.7 eV (C=O), simultaneously indicating highly oxidized GO structure (see Fig. S5. for further information). In particular, the C1s spectra of GO_h-Tpy exhibited the appearance of new prominent peak at 285.8 eV, which can be assigned to C-N bonds. An increase in the intensity of the peak C-C (284.4 eV) at C1s of GO_h-Tpy (Fig S5i) confirms the connection of GO with Tpy . Additionally, a significant decrease of peak attributed to C-O on Fig. S5g-i bonds implies the main functionalization route is the epoxide ring opening reaction. Noteworthy, the successful functionalization of GO with Tpy is proved by the N1s spectra (Fig. S5h). The high-resolution N1s spectra of GO and GO_h samples do not show any nitrogen signal (Fig. S5b,d), whereas the N1s spectra of GO-Tpy and GO_h-Tpy can be deconvoluted into three peaks at 398.8 eV, 399.5 eV, 402.2 eV which can be ascribed to C=N, C-NH-C, and NH_3^+, respectively (Fig. S5h).[62-64] The protonated amines (NH_3^+) can cooperate in the functionalization process by means of electrostatic interactions with deprotonated carboxylic subunits. Moreover, the amount of N-C bonds increased due to reaction between NH_2 groups observed on Tpy with epoxy-carbon atoms on surface of GOs.

The morphology and structural features of the GO, GO_h GO-Tpy and GO_h-Tpy hybrids were investigated by scanning electron microscopy (SEM). SEM images of GO and GO_h portrayed in Fig. 2a-b revealed a highly wrinkled structure which facilitates achieving excellent contact with analysed solution. After functionalization of GO and GO_h with Tpy subunit the GO-Tpy and GO_h-Tpy hybrids possess a homogenous 3D porous network structure when compared to the pristine substrates (Fig. 2c-d).

The results of the BET analysis, which is regarded as an effective strategy for investigating the specific surface area of nanomaterials,[65-68] are shown in Fig. 2e. The N_2 adsorption-desorption isotherms measurements at 77 K of as-prepared GO_h-Tpy exhibit typical IV-type isotherms, indicating the presence of mesopores with many slit holes with the average pore diameter calculated with the Barrett-Joyner-Haleda (BJH) model to be 10.4 nm (see table S4 and Fig. S6 in Supporting Information). The specific surface area of GO_h-Tpy amounts to 185 $m^2 g^{-1}$, which is ca. 8 times greater when compared with the specific surface area of the starting material (GO_h - *ca.* 28. $m^2 g^{-1}$), and demonstrates that the Tpy moieties attachment yields an increase in the specific surface area of GO_h. Similar trends were observed for the GO-Tpy hybrid, nonetheless as a result of the lower degree of oxidation of GO, the final specific surface area and average pore diameter decreased of *ca.* 80% and 85% values when compared to GO_h-Tpy system (table S4).

Structural characteristics of the hybrids as well as raw materials were studied by powder X-ray diffraction which is presented on Fig. 2f. The starting materials (GO, GO_h) possess a typical sharp peak at 10.02° corresponding to an interlayer spacing of 0.88 nm due to the 001 reflection of stacked GO sheets. The pristine GO sample possesses two peaks reflected at 2 Θ = 25.94° and 10.02°, corresponding to the ordered (002) hexagonal graphitic planes and (001) defected hexagonal graphitic structure. The increase of oxidation degree results in the disappearance of the peak located at 25.94°, which proves that a large number of oxygen-containing groups have been introduced to the GO sheet. After functionalization process, the inter-layer spacing based on the Bragg equation increased from 0.88 to 1.09 nm, indicating successful introduction of Tpy moieties between the GO sheets.

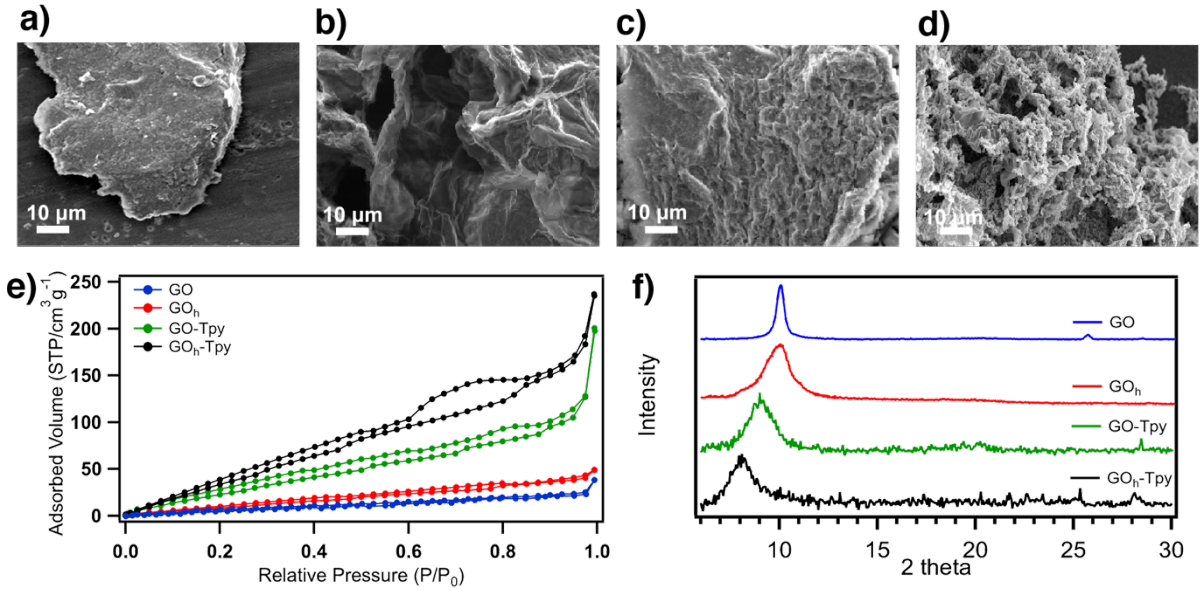

Fig. 2 SEM images displaying the morphology of a) GO, b) GO_h c) GO-Tpy and d) GO_h-Tpy materials; e) BET adsorption-desorption isotherms of the GO, GO_h, GO-Tpy and GO_h-Tpy hybrids; f) Wide-angle X-ray scattering patterns of GO, GO_h GO-Tpy and GO_h-Tpy powders.

The thermal stability of GO, GO_h, Tpy, GO-Tpy and GO_h–Tpy (Fig. S7) was investigated using thermal gravimetric analysis (TGA). The GO_h undergoes a significant weight loss of *ca.* 50% in range of 90–300°C, indicating the decomposition of oxygen functional groups.[69] Tpy is thermally stable up to its melting point of *ca.* 230°C and its decomposition ends at 375°C. Notably, GO_h–Tpy thermal decomposition was found to occur in two steps. First about 90°C indicating the removal of water which amount *ca.* 8% weight loss. Higher drop of mass percentage was monitored around 300°C and it can be associated with the deoxygenation process and Tpy thermal degradation. The results of TGA analysis for GO_h–Tpy hybrid indicate that functionalization of GO with Tpy group is characterized by an increase of the overall thermal stability of the hybrid material, which is a result of the replacement of the less-stable oxygen containing groups at the surface of GO_h with the amine groups coming from Tpy.[41]

Adsorption of metal ions on GO_h-Tpy

To determine the best conditions for the maximum removal of Ni(II), Zn(II), Co(II) ions from aqueous solutions, various adsorption parameters were changed systematically such as pH, the contact time and heavy metal ions concentration. While it is notorious that the pH strongly affects the sorption of heavy metals because it influences the metal species and the charge generated on the adsorbent surface, in our specific case, this susceptibility is even more severe. In fact, the chemistry of our sorbent components, *i.e.* the modified graphene oxide GO_h surface and the grafted Tpy subunit, is particularly sensitive to changes in pH since the scaffold's protonation can markedly modify association constants of their interaction with ions. This mostly affects the oligopyridine scaffold, where the equilibrium between the H^+ cation and heavy metal ions occurs.[70] The effect of pH on the adsorption of Ni(II), Zn(II), Co(II),

onto GO_h-Tpy was plotted in Fig. S8, with the pH values adjusted in the range from 2 to 10. The adsorpion capacity of Ni(II), Zn(II) and Co(II) onto GO_h-Tpy was studied separately for each metal ion and increased quickly in pH range 2-6 to reach the maximum values at pH 6-7, which remained constant and slightly decreased from pH 7 until pH 10 (by ca. 10%). At lower pH, the relatively high H^+ concentration would strongly compete with metal ions for the adsorption sites due to protonation of the hydroxyl and carboxyl groups from the GO_h surface[71] as well as the Tpy subunit itself.[72] This finds reflection in the determination of the pH point of zero charge (pH_{pzc}), which is related to the surface charge properties of the adsorbent.[73] Changes in zeta potential as the function of pH (Fig. S8) show that the pH_{pzc} of the GO_h-Tpy is 4, thus, the deprotonated surface of GO_h-Tpy, favors the adsorption of cationic species when the pH higher than 4. Moreover, the as-prepared GO_h-Tpy is negatively charged in most of natural water environment, hence it is prone to form stable complex compounds with positively charged metal ions interacting with its surfaces.[61] The slight decrease of adsorption of Ni(II), Zn(II) and Co(II) at pH 8-10 can be explained by the formation of hydroxide complexes *e.g.* $NiOH^+$, $ZnOH^+$, $CoOH^+$ (Fig. S9).

Specifically, the unique character of the hybrid material stems from the fact that the sole terpyridine ligands are prone to salting out of the solution in neutral aqueous environment,[72] whereas the GO materials can undergo pH dependent aggregation and/or micellization.[71] Herein, neither of this happens and potent heavy metal ion chemisorption is observed *via* negatively charged carboxylic acid and hydroxyl groups, followed by the N-heterocyclic Tpy moiety. High logK values of Tpy ligand towards heavy metal ions and weak-to-moderate towards alkaline and alkali metal ions also allows a selective binding of the former ones from tap water *vs* alkali and alkaline cations (*vide infra*).[70, 74] In order to obtain high adsorption capacity and to prevent precipitation of the metals in the form of hydroxides which is observed for Ni(II), Zn(II), Co(II) at pH >7 (Fig. S9), further experiments were carried out at pH=6.

Adsorption isotherms

The Langmuir (Eq.3 in experimental section) and Freundlich (Eq.4) adsorption isotherms were used to investigate the maximum adsorption capacity (q_{max}) and to understand the adsorption mechanism of the chosen heavy metal ions (Ni(II), Zn(II), Co(II)) on GO_h-Tpy. For the sake of comparison, control experiments including neat GO, GO_h and GO-Tpy as adsorbents were also carried out and presented on Fig. 3. Isotherm parameters obtained by fitting the Langmuir and Freundlich models are summarized in table S5. Noteworthy, the adsorption isotherms are better fitted by the Langmuir model than by the Freundlich model, suggesting that heavy metal ions adsorption onto the GO, GO_h, GO-Tpy and GO_h-Tpy are adsorbed with homogeneous binding sites, no interaction between adsorbed species, equivalent adsorption energies and monolayer coverage. Furthermore, the *n* constant parameter obtained from Freundlich model is lower than 10, indicating that the sorption process is favourable under studied conditions.[75] Additionally, the XPS measurements were performed for GO_h-Tpy before and after adsorption of Ni(II), Zn(II) and Co(II) metal ions (Fig. S10), which confirm the strong surface complexation between adsorbent and metal species. The q_{max} values of Ni(II), Zn(II), Co(II) on GO_h-Tpy (see table S5) amount to 462, 421 and 336 mg g^{-1}, respectively, being larger than any known sorbents including GO and GO-based sorbents (see table S1). The q_{max} values expressed in mmol g^{-1} amount to 7.9, 6.4 and 5.7 for Ni(II), Zn(II) and Co(II) respectively, suggesting that 1g of GO_h-Tpy is able to adsorb ca. 6 to 8 mmol of divalent heavy metal ions.

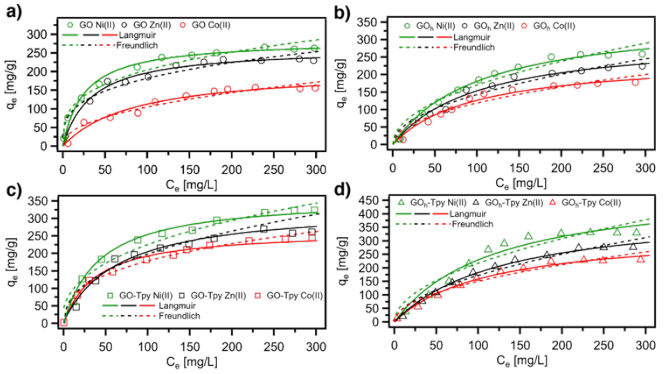

Fig. 3 Adsorption of heavy metal ions as a function of Ni(II), Zn(II), Co(II) concentrations. Uptake isotherms on control samples: a) raw GO, b) highly oxidized GO_h, c) graphene oxide functionalized with terpyridine moieties (GO-Tpy), d) highly oxidized graphene oxide cross linked with terpyridine moieties (GO_h-Tpy). The uptake experiments were carried out at pH=6, ($C_{GO,GOh,GO\text{-}Tpy,GOh\text{-}Tpy}$ = 0.2 g L^{-1}, T=298 K, stirring speed= 200 rpm, t=8 h).

The affinity order of metal ions to the GO_h and GO_h-Tpy hybrid were confirmed by the competitive adsorption using binary and tertiary mixtures (Ni(II)/Zn(II); Zn(II)/Co(II); Ni(II)/Co(II) and Ni(II)/Zn(II)/Co(II)) (Fig. 4a-b), which contained the metal ions solution at pH 6. Notably, the adsorption of Ni(II) was found being the highest in the presence of Zn(II) and Co(II) ions. The experimental data describing affinities of the metal ions toward the GO_h-Tpy follow the order of Ni > Zn > Co. This order agrees very well with first stability constant of the associated metal hydroxides and acetates according to table S6. Moreover, among the studied metal ions, Ni(II) displays the smallest value of ionic radius, facilitating its access in the adsorbents active sites, manifested by the greatest adsorption capacity value. The Tpy logK stability constants follows the following trend: Ni>Co>Zn, which also explains the highest binding of the Ni(II) ions.[72]

Ionic strength can considerably influence the adsorption process of metal ions due to the fact that the number of active functional groups is reduced because of the adsorption of other metal ions. Thus, we have studied the influence of Ni(II), Zn(II) and Co(II) adsorption on GO_h and GO_h-Tpy in the solution of $NaNO_3$ at different concentrations. As shown in fig.S11, even high concentration of background electrolyte (1 mol L^{-1}) does not influence the adsorption of metal ions (Ni(II), Zn(II), Co(II)). Moreover, the Tpy ligands alone precipitate under such condition,[72] which is not the case when they are covalently bound to the graphene oxide matrix.

For the practical application in water remediation, the adsorbent should possess excellent regeneration and recycling performance and should function in the presence of interfering I and II group cations. Real-life application of the GO_h and hybrid GO_h-Tpy sorbent was demonstrated on purification of the drinking (tap) water, which contains alkali (Na(I), K(I)) and alkaline (Mg(II), Ca(II)) metal ions at the following concentrations: 16 mg L^{-1}, 7 mg L^{-1} 10 mg L^{-1} and 75 mg

L^{-1}, respectively. Not only we observed that the single adsorption tests carried out for Ni(II), Zn(II), Co(II) metal ions in the presence of tap water are nearly identical to those obtained for MiliQ water experiments (Fig. 4c-d), but also successful regeneration of the material was demonstrated.

The ability of GO_h and GO_h-Tpy regeneration was evaluated through a series of adsorption-desorption cycles. For each cycle, the hybrid is immersed in the aqueous solution of metal ions at pH 6 and treated with 0.1 M HNO_3. As presented in Fig. 4e-f, the overall decrease in adsorption capacity after ten cycles amounts to 90% (Ni(II), Co(II)) or 95% (Zn(II)) of the initial adsorption capacity, thus providing evidence that GO_h-Tpy hybrid is stable under the experimental process and shows excellent reusability even in comparison with pristine GO_h. The observed behaviour is a result of the choice of the N-heterocyclic terpyridine moiety grafted onto the GO scaffold, which is synergically responsible for the dimensionalization of the system (higher stability and porosity) but also exhibits a few orders of magnitude higher complexes stability constant (logK) towards d-block metal ions vs. alkali and alkaline cations (selectivity).[72]

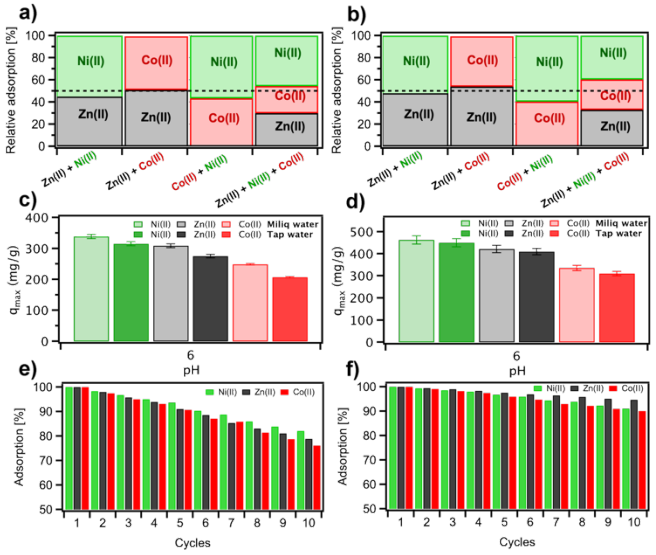

Fig. 4 Multicomponent (binary and ternary) sorption of Ni(II), Zn(II), Co(II) on a) GO_h and b) GO_h-Tpy expressed as a percentage adsorption capacity. The effect of environmental conditions on the adsorption Ni(II), Zn(II) and Co(II) ions by c) GO_h and d) GO_h-Tpy hybrids. Reusability studies of e) GO_h and f) GO_h-Tpy after 10 cycles.

Adsorption kinetics

Since upon functionalization the highly oxidized GO_h incorporates more coordinating Tpy moieties than the GO, the GO_h-Tpy hybrid was chosen for subsequent metal-ion adsorption kinetic and thermodynamic studies. The effect of contact time on the adsorption of Ni(II), Zn(II) and Co(II) ions was investigated and portrayed in Fig. S12a. Compared with GO, where the metal adsorbs after *ca.* 20 min on its surface,[40] the adsorption of heavy metal ions on GO_h-Tpy increases remarkably at the beginning of the experiment and then it reaches a plateau after 180 min, whereas the maximum adsorption capacity is few times higher in comparison to pure GO. The adsorption rate is higher at the beginning due to the fact that greater number of reaction sites is available. According to the above results, the mixing time was fixed at 8 h in the following experiments to make sure that the adsorption reaction can achieve complete equilibrium. To identify the rate-controlling mechanisms during the adsorption of Ni(II), Zn(II) and Co(II), the pseudo-first-order (Fig. S12b), pseudo-second-order (Fig. S12c) and intra-particle diffusion model (Fig. S12d) were applied to estimate the experimental data. The calculated kinetic parameters for adsorption of Ni(II), Zn(II), Co(II) ions at pH=6 are presented in table S7. The percentage adsorption reached 95-97% after 180 min for Ni(II), Zn(II), Co(II). The values of the correlation coefficient as well as the experimental adsorption values (*qe*) determined the applicability of the pseudo-second-order model for describing the experimental data, indicating that the adsorption process is driven by strong complexation of metal ions with the oxygen and nitrogen atoms of GO_h-Tpy (see table S7).

To gain insight into the adsorption process and analyze the rate-determining step of the surface sorption reaction, the intra-particle diffusion model was applied. According to the model, if intraparticle diffusion is the rate limiting step of the entire adsorption process, the plots of q_t *vs* $t^{1/2}$ should yield a straight line passing through the origin of the plot.[76] Fig. S12d shows that the data points are related by two straights lines, the first sharper portion is attributed to the diffusion of adsorbate through the solution to the external surface of the adsorbent (external diffusion) while the second portion describes the gradual adsorption stage, corresponding to the diffusion of adsorbate molecules inside the adsorbent (intra-particle diffusion).[77] The values of k_{p1}, k_{p2}, C_1 and C_2 calculated from the intercept and slope of plot q_t *vs* $t^{1/2}$ are summarized in table S8. The intra-particle diffusion rate constant (k_{p1}) for the first sharper portion is higher than that (k_{p2}) for the second portion, whereas C_1 is lower than C_2, which shows that the rate of Ni(II), Zn(II) and Co(II) removal were higher at the beginning due to large surface area of the adsorbent available for the adsorption of metal ions. After the adsorbent gradually attained equilibrium, the capacity of adsorbent was controlled by the intra-particle diffusion. None of the plots passed through the origin, which indicates that the intra-particle diffusion was part of the adsorption but was not the only rate-controling step.[78] Specifically, binding of cations to the Tpy subunits can happen either in the 1:1 'open' or 2:1 'closed' (Tpy:Me(II)) ratio, while the latter would result in an additional GO matrix folding. Few other mechanisms such as complexation or ion-exchange mechanism may also control the rate of adsorption process.[79]

Adsorption thermodynamics

To further investigate the nature of adsorption process, the thermodynamic behaviour has been studied by comparing the adsorption properties of the GO_h-Tpy at different temperatures. Determination of different thermodynamic parameters, including the Gibbs free energy (ΔG), the entropy (ΔS) and enthalpy (ΔH) changes, was done according to previously presented equations (see Eq. 8-9). The values of ΔH° and ΔS° can be determined from the slope and intercept by plotting the values of $\ln K_c$ *vs.* 1/T (Fig. S13). The obtained ΔG, ΔS and ΔH for the adsorption of Zn(II), Co(II) and Ni(II) ions on the GO_h-Tpy are listed in table S9. The negative values of ΔG° at different temperatures (298-318 K) confirmed the spontaneous nature of the adsorption process. The decreasing ΔG° values with the increasing temperature provide evidence that sorption process may occur more efficiently at higher temperature. The positive values of ΔS° also shows the increment randomness at the surface of

adsorbent during the adsorption process which can be reflected by the affinity of GO_h-Tpy for heavy metal ions and suggested some conformational changes in the GO_h-Tpy structure. On the other hand, the positive value of ΔH° indicates that the adsorption process for GO_h-Tpy is purely based on endothermic process. This result also supports the suggestion that the adsorption capacity of adsorbent increases with the temperature.

Experimental

Reagents and Solutions

Commercially available metal salts, organic compounds and solvents were purchased from Sigma Aldrich or/and Merck Chemical Company (analitycal grade), used without any purification. All solutions were prepared with Mili-Q deionized water. 4-([2,2':6',2''-terpyridin]-4'-yloxy)butan-1-amine (Tpy) was synthesized according to synthetic route described in detail in Supporting Information (see *Experimental section* and Fig. S1).

Synthesis of GO and GO_h

The GOs with different oxidation degrees were synthesized by using modified Hummers method (see *Experimental section* in SI for further information) according to previously published work.[80] GO is generally prepared as stable aqueous dispersion at 4 mg mL^{-1} concentration by treating graphite with the appropriate mass of $KMnO_4$ in H_2SO_4. The different *graphite: $KMnO_4$* ratio introduces various quantities of oxygen atoms on the surface GO in the form of epoxy, hydroxyl and carboxyl groups. Functional groups containing oxygen atoms exhibit an ability to form stable dative bonds with chosen heavy metal ions. We decided to use two different *graphite: $KMnO_4$* ratios (1:1.5 and 1:3 *w:w*) yielding GO with 39.8% and 58.8% oxidation degrees, respectively. The composition of GO and GO_h , which were subsequently used for the synthesis of hybrids, were characterized by various experimental techniques including XPS (see SI for further information).

Preparation of GO-Tpy and GO_h-Tpy

A batch of GO-Tpy and GO_h-Tpy were prepared as follows: a mixture of ethanol (100 mL) and GO or GO_h (100 mL, 4 mg mL^{-1}) was sonicated for 30 min and then 100 mL of previously optimized 2-fold excess of Tpy in ethanol (8 mg mL^{-1}) was added. The mixture was vigorously stirred overnight under reflux. The resulting powder was then filtered and washed several times with water/ethanol mixture (1:1 *vol:vol*). Finally, Soxhlet extraction was used to remove unreacted residuals. The resulting black powder was then freeze-dried for 24 h under vacuum. Preparation of the new hybrids was controlled during the synthesis *via* XPS and elementary analysis (see table S2-3) and its detailed characterization is described in the main text.

Instruments

The morphology of GO, GO_h, GO-Tpy and GO_h-Tpy was analysed by scanning electron microscopy (SEM) using a FEI Quanta 250 FEG instrument. SEM samples were prepared by mounted on carbon conductive tabs followed by gold coating. The composition of GOs as well as GO-based hybrids were characterized with a Thermo Scientific KAlpha x-ray photoelectron spectrometer. The measurements were performed using basic chamber pressure of ~10^{-9} mbar and an Al anode as the X-ray source (X-ray radiation of 1486 eV). Spot sizes of 400 µm were used and pass energies of 200.00 eV for wide energy scans (10 scans) and 10.00-20.00 eV for high-resolution scans (20 scans) were exploited. The ~5 mg of GO, GO_h, GO-Tpy and GO_h-Tpy samples are attached to copper film as powder. The C1s photoelectron binding energy was set at 284.5 ± 0.2 eV and used as a reference for calibrating the other peak positions. For each sample, the analysis was repeated three times. Fourier transform infrared (FTIR) spectra were recorded within the mid-IR range (500–4000 cm^{-1}) by using a Perkin Elmer Spectrometer (Spectrum Two) equipped with ATR Diamond. The hybrid in the form of powder, earlier dried in a freeze dryer was studied at room temperature. The specific surface area was carried out on a Micromeritics ASAP 2050 surface area and porosity analyser. Prior to the Braunauer-Emmett-Teller (BET) method, the samples were outgassed for 10 hours at 100 °C. The specific surface area was determined from adsorption/desorption isotherms of nitrogen at 77 K and pressures up to 1 bar. The zeta potential was measured at various pH by Malvern Zetasizer Nano ZS instrument at room temperature. Thermogravimetric analysis (TGA) were carried out in the temperature range 50-500 °C operating under ambient condition, with a ramp of 10 °C/min on a Mettler Toledo TGA/SDTA851e system. Raman spectra were measured at room temperature by Renishaw microscope with a 100x objective, laser excitation wavelength of 532 nm and laser power of 0.05%. The silicon peak at 520.3 cm^{-1} was took as reference for wavenumber calibration. The D and G peaks were fitted with combined Gaussian and Lorentzian functions. X-ray powder diffraction (XRD) data were collected on powder specimens using Bruker ASX D8 Advanced equipped with Cu anode with Kα radiation (λ = 1.5418 Å). Diffraction patterns were collected at room temperature in the scattered angular range between 6° and 30° with an angular resolution of 0.02° per step and a typical counting time 4 of 10 s per step. Nuclear magnetic resonance (^{1}H NMR) were recorded on a Mercury-plus-300 MHz spectrometer and calibrated against the residual protonated solvent signals ($CDCl_3$: δ = 7.26), given in *ppm*. Elemental analyses were performed by Perkin Elmer 2400II. The concentration of metal ions was determined using flame atomic absorption spectrometry (F-AAS) with deuterium arc background correction, equipped with a hollow cathode lamp. An air–acetylene burner was used. The wavelengths (spectral band pass) were 213.86 nm, 230.79 nm and 231.60 nm for Zn(II), Ni(II) and Co(II), respectively. The nebulizer flow rate was set to 5.0 mL min^{-1}.

Conclusions

In summary, we have reported the synthesis of a novel 3D GO_h-Tpy hybrid by means of a facile and effective covalent bond formation. Compared to the as-prepared GO, GO_h and GO-Tpy, the GO_h-Tpy adsorbent exhibited the highest adsorption efficiency of heavy metal ions due to synergist contribution of GO_h and Tpy components. The maximum adsorption capacities (q_{max}) of GO_h-Tpy system fitted by Langmuir isotherm model for Ni(II), Zn(II) and Co(II) are achieved at pH=6 reaching 462, 421 and 336 mg g^{-1}, respectively, being the highest reported values in the literature including pristine GO and GO-based sorbents. The adsorption of Ni(II), Zn(II) and Co(II) was described well

using the pseudo-second-order kinetic model, indicating that the process is driven by strong complexation of metal ions with the oxygen (GO_h) and nitrogen (Tpy) atoms present in the hybride. GO_h-Tpy exhibits outstanding remediation performance towards heavy metal ions (Ni(II), Zn(II), Co(II)), attributed to its high surface-to-volume ratio and interconnected pore network in the 3D architecture. Specifically, a selective sorption of alkali and alkaline metal ions from the drinking water samples was demonstrated, followed by desirable cycling stability, reusability and ease of separation operation of the GO_h-Tpy hybrid, paving the way towards application of this type of adsorbents in real-life wastewater purification processes.

Conflicts of interest

The authors declare no competing financial interest.

Acknowledgements

This work was supported by the National Science Centre (Grant no. 2017/27/N/ST5/00173) D.P acknowledges the support from the Embassy of France in Poland in the form of scholarship at the Institut de Science et d'Ingénierie Supramoléculaires, University of Strasbourg. Additionally, D.P. acknowledge the support from Foundation for Polish Science (FNP) in the form of scholarship. A.G. Foundation for Polish Science (FNP) in the form of scholarship is gratefully acknowledged. Y.N. acknowledge JSPS KAKENHI (20H05224) for finantial support. We also acknowledge funding from European Commission through the ERC Proof-of-Concept project GRAPHEME (GA-899596), the Graphene Flagship Core 3 project (GA-881603), the Agence Nationale de la Recherche through the Labex project CSC (ANR-10-LABX-0026 CSC) within the Investissement d'Avenir program (ANR-10-120 IDEX-0002-02), the International Center for Frontier Research in Chemistry (icFRC) as well as the Institut Universitaire de France (IUF).

References

1. J. B. Zimmerman, P. T. Anastas, H. C. Erythropel and W. Leitner, *Science*, 2020, **367**, 397-400.
2. M. Z. Jacobson, *Energy Environ. Sci.*, 2009, **2**, 148-173.
3. F. Fu and Q. Wang, *J. Environ. Manage.*, 2011, **92**, 407-418.
4. R. P. Schwarzenbach, T. Egli, T. B. Hofstetter, U. v. Gunten and B. Wehrli, *Annu. Rev. Environ. Resour.*, 2010, **35**, 109-136.
5. B. Dhal, H. N. Thatoi, N. N. Das and B. D. Pandey, *J. Hazard. Mater.*, 2013, **250-251**, 272-291.
6. N. Rascio and F. Navari-Izzo, *Plant Science*, 2011, **180**, 169-181.
7. P. C. Nagajyoti, K. D. Lee and T. V. M. Sreekanth, *Environ. Chem. Lett.*, 2010, **8**, 199-216.
8. L. Järup, *Br. Med. Bull.* , 2003, **68**, 167-182.
9. P. B. Tchounwou, C. G. Yedjou, A. K. Patlolla and D. J. Sutton, in *Molecular, Clinical and Environmental Toxicology*, ed. A. Luch, Springer Basel, Basel, 2012, pp. 133-164.
10. N. Zhang, W. Qi, L. Huang, E. Jiang, J. Bao, X. Zhang, B. An and G. He, *Chin. J. Chem. Eng.*, 2019, **27**, 1348-1360.
11. J. Park, P. Bazylewski and G. Fanchini, *Nanoscale*, 2016, **8**, 9563-9571.
12. S. Wadhawan, A. Jain, J. Nayyar and S. K. Mehta, *J. Water Process. Eng.*, 2020, **33**, 101038.
13. X. Liu, R. Ma, X. Wang, Y. Ma, Y. Yang, L. Zhuang, S. Zhang, R. Jehan, J. Chen and X. Wang, *Environ. Pollut.*, 2019, **252**, 62-73.
14. S. Remanan, N. Padmavathy, S. Ghosh, S. Mondal, S. Bose and N. C. Das, *Sep. Purif. Rev.*, 2020, 1-21.
15. S. Babel and T. A. Kurniawan, *J. Hazard. Mater.*, 2003, **97**, 219-243.
16. T. Kouznetsova, A. Ivanets, V. Prozorovich, A. Hosseini-Bandegharaei, H. N. Tran, V. Srivastava and M. Sillanpää, *Wat. Sci. Technol.*, 2020, **82**, 984-997.
17. A. Alsbaiee, B. J. Smith, L. Xiao, Y. Ling, D. E. Helbling and W. R. Dichtel, *Nature*, 2016, **529**, 190-194.
18. Z. Reddad, C. Gerente, Y. Andres and P. L. Cloirec, *Environ. Technol.*, 2003, **24**, 257-264.
19. S. Milićević, V. Milošević, D. Povrenović, J. Stojanović, S. Martinović and B. Babić, *Clays Clay Miner.*, 2013, **61**, 508-516.
20. G. Crini, *Bioresour. Technol.*, 2006, **97**, 1061-1085.
21. X. Qu, P. J. J. Alvarez and Q. Li, *Water Res.*, 2013, **47**, 3931-3946.
22. H. N. Tran, H. C. Nguyen, S. H. Woo, T. V. Nguyen, S. Vigneswaran, A. Hosseini-Bandegharaei, J. Rinklebe, A. Kumar Sarmah, A. Ivanets, G. L. Dotto, T. T. Bui, R.-S. Juang and H.-P. Chao, *Crit. Rev. Env. Sci. Tec.* , 2019, **49**, 2155-2219.
23. H. N. Tran and H.-P. Chao, *Environ. Sci. Pollut. Res.*, 2018, **25**, 12808-12820.
24. S. Yang, J. Li, D. Shao, J. Hu and X. Wang, *Journal of Hazardous Materials*, 2009, **166**, 109-116.
25. C. Xu, C. Jiao, R. Yao, A. Lin and W. Jiao, *Environ. Pollut.*, 2018, **233**, 194-200.
26. Z. Lin, Y. Hu, Y. Yuan, B. Hu and B. Wang, *Ecotoxicol. Environ. Saf.*, 2021, **208**, 111451.
27. X. Liu, H. Pang, X. Liu, Q. Li, N. Zhang, L. Mao, M. Qiu, B. Hu, H. Yang and X. Wang, *The Innovation*, 2021, **2**, 100076.
28. S. Chowdhury and R. Balasubramanian, *Adv. Colloid Interface Sci.*, 2014, **204**, 35-56.
29. F. Perreault, A. Fonseca de Faria and M. Elimelech, *Chem. Soc. Rev.*, 2015, **44**, 5861-5896.
30. S. C. Smith and D. F. Rodrigues, *Carbon*, 2015, **91**, 122-143.
31. I. Ali, A. A. Basheer, X. Y. Mbianda, A. Burakov, E. Galunin, I. Burakova, E. Mkrtchyan, A. Tkachev and V. Grachev, *Environ. Int.*, 2019, **127**, 160-180.
32. D. H. Seo, S. Pineda, Y. C. Woo, M. Xie, A. T. Murdock, E. Y. M. Ang, Y. Jiao, M. J. Park, S. I. Lim, M. Lawn, F. F. Borghi, Z. J. Han, S. Gray, G. Millar, A. Du, H. K. Shon, T. Y. Ng and K. Ostrikov, *Nta. Commun.*, 2018, **9**, 683.
33. G. Bottari, M. Á. Herranz, L. Wibmer, M. Volland, L. Rodríguez-Pérez, D. M. Guldi, A. Hirsch, N. Martín, F. D'Souza and T. Torres, *Chem. Soc. Rev.*, 2017, **46**, 4464-4500.
34. S. Navalón, J. R. Herance, M. Álvaro and H. García, *Chem. Eur. J.*, 2017, **23**, 15244-15275.
35. P. Samaddar, Y.-S. Son, D. C. W. Tsang, K.-H. Kim and S. Kumar, *Coord. Chem. Rev.*, 2018, **368**, 93-114.
36. W. Peng, H. Li, Y. Liu and S. Song, *J. Mol. Liq.*, 2017, **230**, 496-504.
37. S. Yang, C. Chen, Y. Chen, J. Li, D. Wang, X. Wang and W. Hu, *ChemPlusChem*, 2015, **80**, 480-484.
38. R. Zare-Dorabei, S. M. Ferdowsi, A. Barzin and A. Tadjarodi, *Ultrason. Sonochem.*, 2016, **32**, 265-276.
39. G. Sheng, C. Huang, G. Chen, J. Sheng, X. Ren, B. Hu, J. Ma, X. Wang, Y. Huang, A. Alsaedi and T. Hayat, *Environ. Pollut.*, 2018, **233**, 125-131.
40. R. Sitko, E. Turek, B. Zawisza, E. Malicka, E. Talik, J. Heimann, A. Gagor, B. Feist and R. Wrzalik, *Dalton Trans.*, 2013, **42**, 5682-5689.
41. M. Ramezanzadeh, M. Asghari, B. Ramezanzadeh and G. Bahlakeh, *Chem. Eng. J.*, 2018, **337**, 385-397.
42. L. P. Lingamdinne, J. R. Koduru, H. Roh, Y.-L. Choi, Y.-Y. Chang and J.-K. Yang, *Hydrometallurgy*, 2016, **165**, 90-96.
43. F. Fang, L. Kong, J. Huang, S. Wu, K. Zhang, X. Wang, B. Sun, Z. Jin, J. Wang, X.-J. Huang and J. Liu, *J. Hazard. Mater.*, 2014, **270**, 1-10.
44. C. Zolezzi, C. F. Ihle, C. Angulo, P. Palma and H. Palza, *Ind. Eng. Chem. Res.*, 2018, **57**, 15722-15730.
45. M. M. Kadam, O. R. Lokare, K. V. M. K. Kireeti, V. G. Gaikar and N. Jha, *RSC Adv.*, 2014, **4**, 62737-62745.
46. A. Dąbrowski, *Adv. Colloid Interface Sci.*, 2001, **93**, 135-224.
47. R. D. Hancock, *Chemical Society Reviews*, 2013, **42**, 1500-1524.
48. A. Gorczyński, J. M. Harrowfield, V. Patroniak and A. R. Stefankiewicz, *Chemical Reviews*, 2016, **116**, 14620-14674.
49. S. Chakraborty and G. R. Newkome, *Chem. Soc. Rev.*, 2018, **47**, 3991-4016.
50. H. Hofmeier and U. S. Schubert, *Chem. Soc. Rev.*, 2004, **33**, 373-399.
51. J. Ding, H. Zhao, Z. Shao and H. Yu, *ACS Appl. Mater. Interfaces*, 2019, **11**, 42646-42653.
52. D. Zhou, Q.-Y. Cheng, Y. Cui, T. Wang, X. Li and B.-H. Han, *Carbon*, 2014, **66**, 592-598.
53. S. Song, Y. Xue, L. Feng, H. Elbatal, P. Wang, C. N. Moorefield, G. R. Newkome and L. Dai, *Angew. Chem. Int. Ed.*, 2014, **53**, 1415-1419.
54. X. Zhou, T. Zhang, C. W. Abney, Z. Li and W. Lin, *ACS Appl. Mater. Interfaces*, 2014, **6**, 18475-18479.
55. T. Szabó, T. Szabó-Plánka, D. Jónás, N. V. Nagy, A. Rockenbauer and I. Dékány, *Carbon*, 2014, **72**, 425-428.
56. Y. Chen, X. Zhang, D. Zhang, P. Yu and Y. Ma, *Carbon*, 2011, **49**, 573-580.

57. D. Zhao, X. Gao, C. Wu, R. Xie, S. Feng and C. Chen, *Appl. Surf. Sci.*, 2016, **384**, 1-9.
58. A. C. Ferrari and D. M. Basko, *Nat. Nanotech.*, 2013, **8**, 235-246.
59. J. Liu, X. Ge, X. Ye, G. Wang, H. Zhang, H. Zhou, Y. Zhang and H. Zhao, *J. Mat. Chem. A*, 2016, **4**, 1970-1979.
60. X. Dong, X. Wang, J. Wang, H. Song, X. Li, L. Wang, M. B. Chan-Park, C. M. Li and P. Chen, *Carbon*, 2012, **50**, 4865-4870.
61. X. Zhang, A. Ciesielski, F. Richard, P. Chen, E. A. Prasetyanto, L. De Cola and P. Samorì, *Small*, 2016, **12**, 1044-1052.
62. A. Calborean, F. Martin, D. Marconi, R. Turcu, I. E. Kacso, L. Buimaga-Iarinca, F. Graur and I. Turcu, *Mater. Sci. Eng.*, 2015, **57**, 171-180.
63. F. Zhao, E. Repo, Y. Song, D. Yin, S. B. Hammouda, L. Chen, S. Kalliola, J. Tang, K. C. Tam and M. Sillanpää, *Green Chem.*, 2017, **19**, 4816-4828.
64. F. A. Martin, D. Marconi, S. Neamtu, T. Radu, M. Florescu, R. Turcu, C. Lar, N. D. Hădade, I. Grosu and I. Turcu, *Mater. Sci. Eng. C*, 2017, **75**, 1343-1350.
65. H. X. Zhong, J. Wang, Y. W. Zhang, W. L. Xu, W. Xing, D. Xu, Y. F. Zhang and X. B. Zhang, *Angew. Chem. Int. Ed.*, 2014, **53**, 14235-14239.
66. R. Dash, J. Chmiola, G. Yushin, Y. Gogotsi, G. Laudisio, J. Singer, J. Fischer and S. Kucheyev, *Carbon*, 2006, **44**, 2489-2497.
67. B. Song, C. Sizemore, L. Li, X. Huang, Z. Lin, K.-s. Moon and C.-P. Wong, *J. Mat. Chem. A*, 2015, **3**, 21789-21796.
68. Q. Fu, L. Zhang, H. Zhang, X. Chen, M. Li and M. Gong, *Environ. Res.*, 2020, **186**, 109608.
69. X. Zhang, Y. Huang, Y. Wang, Y. Ma, Z. Liu and Y. Chen, *Carbon*, 2009, **47**, 334-337.
70. R. D. Hancock, *Chem. Soc. Rev.*, 2013, **42**, 1500-1524.
71. C.-J. Shih, S. Lin, R. Sharma, M. S. Strano and D. Blankschtein, *Langmuir*, 2012, **28**, 235-241.
72. J. M. Hamilton, M. J. Anhorn, K. A. Oscarson, J. H. Reibenspies and R. D. Hancock, *Inorg. Chem.*, 2011, **50**, 2764-2770.
73. L. Cui, Y. Wang, L. Gao, L. Hu, L. Yan, Q. Wei and B. Du, *Chem. Eng. J.*, 2015, **281**, 1-10.
74. R. D. Hancock and A. E. Martell, *Chem. Rev.*, 1989, **89**, 1875-1914.
75. B. H. Hameed, *J. Hazard. Mater.*, 2008, **154**, 204-212.
76. K. Thakur and B. Kandasubramanian, *J. Chem. Eng.* , 2019, **64**, 833-867.
77. S. Figaro, J. P. Avril, F. Brouers, A. Ouensanga and S. Gaspard, *J. Hazard. Mater.*, 2009, **161**, 649-656.
78. X. Mi, G. Huang, W. Xie, W. Wang, Y. Liu and J. Gao, *Carbon*, 2012, **50**, 4856-4864.
79. Y. Liu, Q. Zhao, G. Cheng and H. Xu, *Chem. Eng. J.*, 2011, **173**, 792-800.
80. N. Morimoto, T. Kubo and Y. Nishina, *Sci. Rep.* , 2016, **6**, 21715.